



Contents lists available at ScienceDirect

International Journal of Refractory Metals & Hard Materials

journal homepage: www.elsevier.com/locate/IJRMHM

Perspectives of metal-diamond composites additive manufacturing using SLM-SPS and other techniques for increased wear-impact resistance

Ramin Rahmani^{a,b,*}, Miha Brojan^b, Maksim Antonov^a, Konda Gokuldoss Prashanth^{a,c,d}^a Department of Mechanical and Industrial Engineering, Tallinn University of Technology, Ehitajate tee 5, 19086 Tallinn, Estonia^b Laboratory for Nonlinear Mechanics, Faculty of Mechanical Engineering, University of Ljubljana, Askerceva 6, SI-1000 Ljubljana, Slovenia^c Erich Schmid Institute of Materials Science, Austrian Academy of Science, Jahnstraße 12, A-8700 Leoben, Austria^d CBCMT, School of Mechanical Engineering, Vellore Institute of Technology, 632014, Tamil Nadu, India

ARTICLE INFO

Keywords:

Selective laser melting
 Spark plasma sintering
 Hard material 3D printing
 Metal-diamond powders
 Wear-impact resistance
 Finite element simulation

ABSTRACT

In this paper, a new route is introduced to fabricate parts with increased wear and impact resistance for use in tunneling and mining applications. A combination of selective laser melting (SLM) and spark plasma sintering (SPS) to 3D print functionally graded lattices (FGL) that are later filled with metal-diamond composites was used. It was demonstrated that a cellular lattice plays an important role in the consolidation of diamond particles. Impact-abrasive laboratory experiments with tribological device, developed in-house, were carried out to characterize the fabricated samples. The results show that the balance of nickel, molybdenum, and chromium significantly affects the performance of the fabricated specimens. The addition of a higher content of Mo–Cr, Ni and coated diamond particles guarantees higher impact-abrasive resistance of the composite. Our experimental results show that the FGL structure allows a more accurate distribution of diamond particles (variable metal/refractory material content) across the structure and our finite element simulations showed increased ductility and impact absorption ability due to a more uniform distribution of stresses throughout the volume.

1. Introduction

Additive manufacturing has an immense potential to assist in the development of new classes of materials with precisely engineered microstructures that can work in extremely harsh conditions. For example, a combination of selective laser melting (SLM) of metals and spark plasma sintering (SPS) of metallic, ceramic or composite materials enables the production of composites using functionally graded lattice (FGL) structures with continuous metal lattices for optimized strength and sintered/embedded hard reinforcements for optimized hardness [1,2]. A cost-efficient drag bit for deep geothermal drilling or tunnel boring machines [3] in which harsh impact-abrasive conditions apply is an excellent example of application to test the limits of additive manufacturing (AM) methods, such as 3D printing of metallic and composite materials with diamond inclusions [4,5].

SLM is a rapid prototyping technology based on the powder bed fusion process with the high heating and cooling rate (10^4 – 10^6 K/s [6]) that enables the creation of complicated parts and assemblies directly from computer-aided design (CAD) models. The feeding mechanism is used to deposit agglomerated powders in front of a rubber wiper that sweeps the powder on the building area to form a thin uniform layer.

The minimal possible thickness of the spread layer depends on flowability, sphericity and wiper height adjustment. The laser then pulses and heats the powder on the building area to form a solid object. With this system, the objects are built layer by layer on e.g. Ti6Al4V platform with the help of a servomotor driven elevator that moves downwards by a distance equal to the layer thickness and after every wiping and sintering sequence. The process is carried out in an argon protective environment with a pressure of 6 mbar and an oxygen level < 0.5% [7]. Powders are deposited, melted and consolidated layer by layer with the prescribed thickness (e.g. 0.25–0.5 μ m for SLM50) to manufacture dense layers and CAD designed dimensions. The basis of the SLM classification is usually platform sizes e.g. SLM50, SLM280 or SLM500 (that corresponds to 50, 280 and 500 mm and is prescribing the maximum size of the object that is possible to print) [8]. Unmelted/non-consolidated powders outside the platform, wiped out during the job or after finishing the job can be recycled which is an advantage of AM technology regarding powder consumption [9]. Another benefit of SLM is the ability to use a wide scope of metal, ranging from Ti-, Fe-, Al-, Ni-, Co- to Cu-based powders [10]. Parts fabricated by this technology show better fatigue resistance, fracture toughness and tribological properties compared to their cast counterparts [11].

* Corresponding author at: Department of Mechanical and Industrial Engineering, Tallinn University of Technology, Ehitajate tee 5, 19086 Tallinn, Estonia
 E-mail addresses: ramin.rahmaniahranjani@taltech.ee, ramin.rahmaniahranjani@gmail.com (R. Rahmani).

<https://doi.org/10.1016/j.ijrmhm.2020.105192>

Received 18 December 2019; Accepted 9 January 2020

Available online 10 January 2020

0263-4368/ © 2020 Elsevier Ltd. All rights reserved.

The SPS process is a relatively new solid consolidation sintering technique with simultaneous application of a low voltage, high pulse current, and uniaxial pressure-assisted punch electrodes. The key advantages of this new sintering method over the hot isostatic pressing (HIP) method include very high densities obtained in a short time and a wide-ranging sintering temperature (300–2200 °C), fast heating rate (1000 °C/min) and cooling rate (300 °C/min) compared to the conventional powder metallurgy, e.g. hot isostatic pressing. The DC pulsed electrical direct current in a vacuum chamber generates the spark discharge and rapid Joule heating through graphite mold and powder compact (tungsten carbide molds can be used for hard materials powders) [12,13]. The graphite molds and punches control pressure, as well as thermocouple control (TC) or pyrometer control (PC), applies temperature precise control [14]. SPS is developed for the consolidation of a wide range of different materials, such as metals, ceramics, and composites in different dimensions (usually disk-shaped) and with high density.

The flowability (sphericity), particle size (nano or micro), density, composition, melting points, avalanche angles, inter-particle forces, powder surface fractal, etc., give valuable information about the applicability of powders [15]. For example, due to its high strength-to-weight ratio argon atomized Ti6Al4V powder is widely used in bio-material, aerospace and additive manufacturing applications [16]. Grade 5 titanium alloy containing 5.5–6.75 wt% aluminum and 3.5–4.5 wt% vanadium with 4.43 g/cm³, particle size ≤45 μm and melting point ≥1604 °C has excellent strength, low density and high corrosion resistance. The 316 L powder (with density 7.95 g/cm³) is an austenitic low-carbon non-magnetic stainless steel containing 16–18 wt % chromium, 10–14 wt% nickel and 2–3 wt% molybdenum. Apart from its biomedical and chemical applications, it is outstanding for its excellent fluidity (of powder) in an SLM approach, corrosion resistance and strength at high temperature [17]. Excellent mechanical properties and corrosion resistance of 316 L and Ti6Al4V alloys motivated the researchers to mix them and promote their characteristics [18–21].

Printing diamond particles remains a big challenge. So far, it is only reported as a patent [22]. However, printing diamond particles mixed with metals is already possible, but still in progress [2,23,24]. One such route is via metal-coated polycrystalline diamond (PCD) which is also used in our study [25,26]. The coating usually consists of cobalt, nickel,

aluminum and copper, and a wide variety of carbides, nitrides, ceramics and metal alloys. It is commonly used for its good thermal conductivity in electronic components and in applications where wear resistance is important [27,28]. It was shown, for example, that 316 L-diamond lattice printed structures or sintered diamond along with Ti6Al4V lattice via SPS route has provided uniform distribution of diamond particles and consequently lower wear rates and improved crack resistance [23].

In this paper, we show a novel approach for printing diamond included lattice/matrix structures for the potential use in tunneling and mining applications. We apply a combination of SLM and SPS techniques and propose an axial FGL structure with a dense metal region at the bottom for better weldability/ductility, gradient interlayer filled Ti6Al4V-diamond composite and plain Ni-coated diamond at the top for higher hardness to improve wear-impact resistance. To analyze the influence of the geometry we vary the cell size, strut diameter and volume fraction of the specimen. We show that a cellular lattice structure plays an important role in the consolidation of diamond particles. By introducing a lattice structure, the diamond particles are kept in situ as oppose to the solid printing the 316 L-diamond composite which induces depositions of diamond particles at the bottom of each layer. Nitriding (and/or carburizing), chromium coating, blasting/cleaning by alumina nanopowders, diamond mixing is applied in the recent study as metallic lattice structures post-processing after SLM route. The impact-abrasion tribo-device (IATD), 3D optical surface profiler (OSP), scanning electron microscopy (SEM) and energy-dispersive spectroscopy (EDS) were applied to estimate how well the produced materials can withstand the wear and impact conditions. Demonstration of impact resistance of the specimen in distinct conditions (plain and lattice-included samples) is presented also via finite element simulations.

2. Methods and materials

Functionally graded cellular metallic lattices manufactured by SLM and filled with diamond particles or WC-Co hardmaterials which are sintered with the SPS are proposed to fabricate parts with improved abrasion and impact resistance. A sketch of such FGL structure with a dense metal region at the bottom for better weldability/ductility,

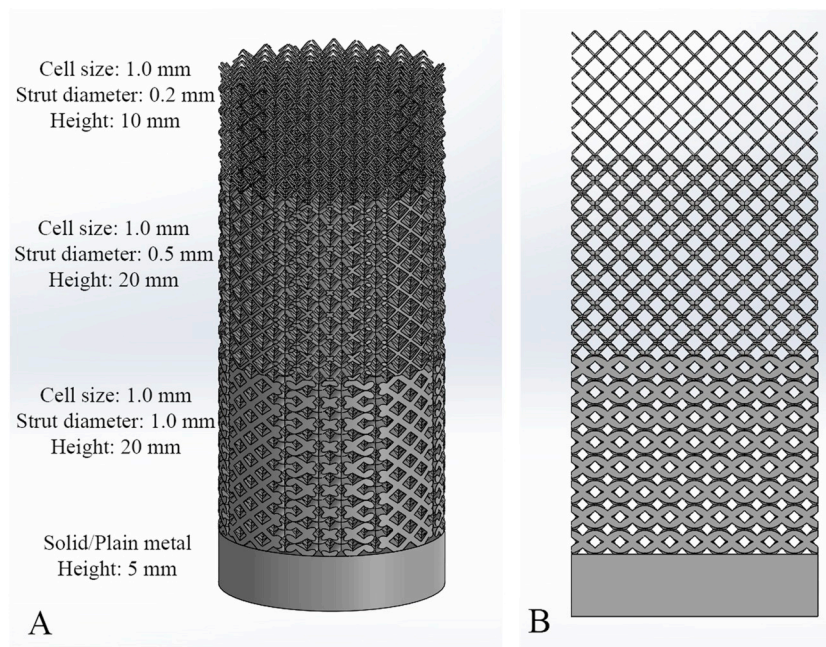


Fig. 1. FGL structure with a dense metal region at the bottom for better weldability/ductility, interlayers gradient metallic and wear resistant at the top. A) Sample with 20 mm diameter proper for SPS mold, B) cross sectional view.

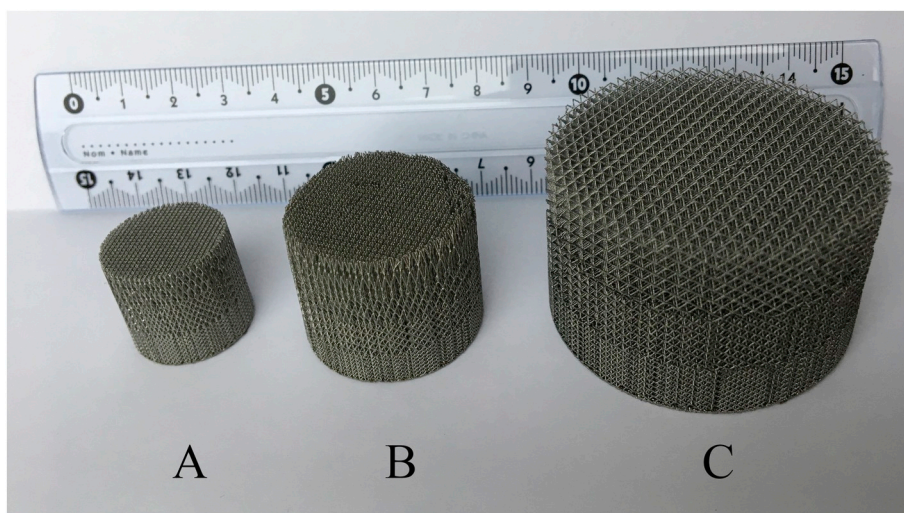


Fig. 2. Demonstration of the possibility of fabrication of Ti6Al4V lattices of required size functionally graded from bottom to top in three volume fraction stages (42, 30, and 16%). The diameters and heights of samples are: A) $\text{Ø}20 \times 18$ mm, B) $\text{Ø}30 \times 24$ mm, C) $\text{Ø}50 \times 30$ mm.

gradient interlayers (metal-ceramic composite) and wear resistant (high hardness) in top is depicted in Fig. 1.

These scaffolds can be filled with various types of hard materials, ceramics, metals or oxides for biocompatibility, antibacterial and tribological applications [29–32]. In Fig. 2, we show three fabricated functionally graded lattices (FGL) made from Ti6Al4V by the SLM technique. The structure of the specimens is denser (higher volume fraction) at the bottom and decreases in three stages towards the top, with 42%, 30% and 16% volume fraction of metal respectively. The outer dimensions of the specimens are given in the figure caption.

Fig. 3 shows four structures made from the same material and the same printing technique with a continuous cell size across the whole specimen. The first two specimens have the same strut diameter and different cell size, whereas the last two have the same cell size but different strut diameter. All the specimens shown in this figure were nitrided in a vacuum nitriding furnace (VNF, under nitrogen gas flowing with $10^\circ\text{C}/\text{min}$ heating rate and 90 min holding time at 900°C) to fabricate TiN phase surrounded lattice beams [23,33]. It is known that, nitrided Ti6Al4V scaffolds have higher brittleness and collapse under lower load; therefore, it is preferred mainly for applications with

followed filling by additional powder and sintering [23,33]. As nitriding takes place in a furnace with constant Ni-flow, the depth of treated material during the process is independent from the volume fraction of Ti6Al4V.

On the other hand, the process of chrome plating via chemical vapor deposition (CVD) is influenced by volume fraction of lattice material. In Fig. 4 three specimens with various lattice cell sizes made from 316 L powder are shown. Even though the CVD reactor conditions were constant for all samples, it is evident that chromium deposition/penetration through the lattice struts is not complete for the specimen with smaller cell sizes (i.e. for higher material volume fractions). Note that with the chrome plating process the metal is protected against corrosion and fatigue and remains sufficiently ductile.

Both metal alloys Ti6Al4V and 316 L used to print the specimens in Figs. 2-4 are ductile scaffolds. With the same technology, it is possible to print also hard materials. For example, one can print Rockit 701 powder, produced by Hoganäs [4], with the element composition Fe 76.3%, W 9.5%, Cr 4%, Nb 1.6%, C 1%, Ti 0.6% and 7% other elements (SEM image of the particles is shown in Fig. 5A). It is convenient for printing impact, abrasive and crack resistant products. Apart from

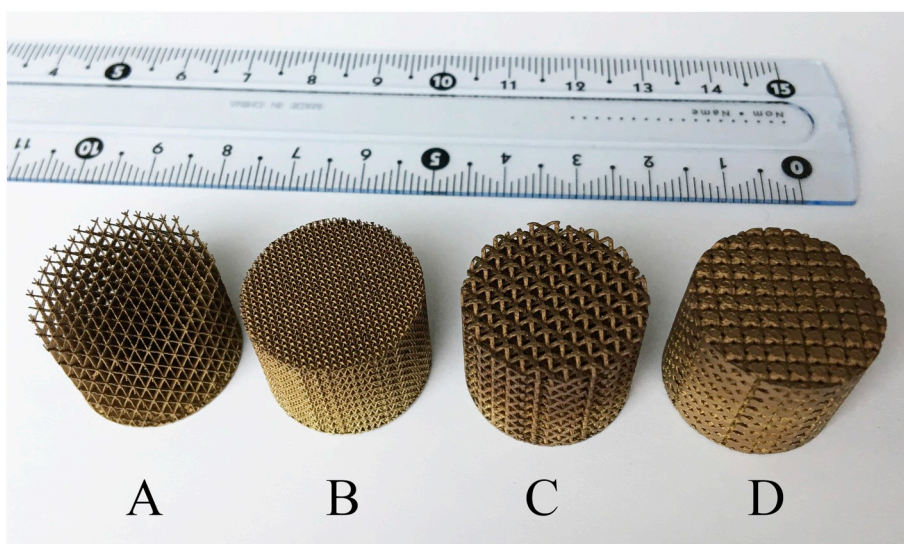


Fig. 3. Nitrided Ti6Al4V lattice structures with varied cell size, strut diameter and approx. Volume fraction: A) 1.5 mm, 0.2 mm, 12%, B) 0.75 mm, 0.2 mm, 26%, C) 1 mm, 0.5 mm, 36%, D) 1 mm, 1 mm, 60%, respectively. All specimens have 20 mm diameter and 15 mm height.

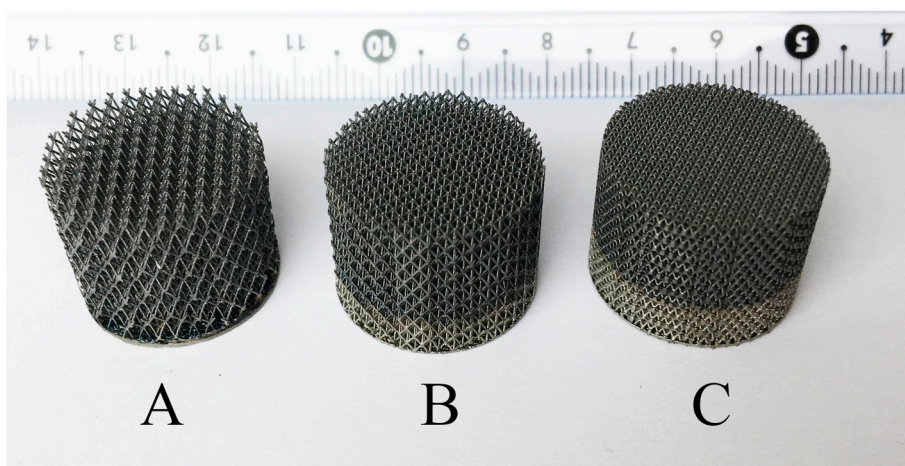


Fig. 4. Chrome plated 316 L lattice structures with varied cell sizes and volume fraction: A) 1.5 mm and 12%, B) 1.0 mm and 19%, and C) 0.75 mm and 26%. The specimens are 20 mm in diameter and 15 mm in height.

sintering tungsten inside 316 L scaffolds, direct 3D printing of Fe-9.5 wt % W is already feasible for consolidating hardmaterial particles in favorable places (see for instance Fig. 5B).

Moreover, it is also possible to consolidate diamond particles in situ [2,23,24]. 3D printed struts with mixture of Ti6Al4V and diamond with 5 wt% of diamond and 10 wt% of diamond are shown in Fig. 6A and B. In the case of 10 wt% diamond mixture, the connection/cohesion of the struts is relatively weak (due to weaker bonding between diamond and metals) which leads to a more brittle scaffold structure. The problem can be solved by increasing the strut diameter. As shown in Fig. 7, the diamond particles are accumulated at the bottom of the strut (due to polygon shape of diamond-nickel particles and spherical shape of Ti6Al4V or 316 L, difference in weight/density/size, and sweeping by printer rubber). Another explanation is that diamond particles in the upper part of layer are destroyed (exploded) by intensive heating and only particles that are at the bottom of the layer are mostly surviving during heating by laser. Therefore, better bonding and homogeneous distribution of diamond particles are expected in a bulk print. This agrees with Fig. 8 where we show a surface of the 3D printed bulk/plain piece.

The 3D printed Ti6Al4V scaffold's surface could be treated by the alumina nanoparticle blasting. The results of the process are shown in Figs. 9 and 10 for different strut diameters (pore sizes). Then, post-cleaning or post-polishing has a pivotal role to avoid single inclusions weakly adhered to main cell structure that is especially important for bio applications with precisely defined pore or strut dimensions [34–36].

Diamond particle sizes, metal coating and fraction of Ti6Al4V have vital roles for full consolidation and to avoid the graphitization as much as SPS parameters (sintering time, temperature, pressure) allow. As

illustrated in XRD pattern in Fig. 11, graphite phase formation is inevitable and can alter to different final constituents; but choosing larger diamond particles with thicker nickel-coating yields better results [2,23]. According to previous findings stated above, the most suitable conditions/materials/processing were selected for current research.

Titanium Ti6Al4V argon atomized powder 5–40 μm (Fig. 12A) and stainless steel AISI 316 L 30–55 μm powder (Fig. 12B), manufactured by TLS Technik GmbH from Germany and Sandvik Osprey Ltd. from UK, respectively, and were used for the cellular lattice structures fabrication. For fabrication of matrices, the following powders were used: chromium metal powder in 6 μm particle size (Fig. 12C) and molybdenum in 1–3 μm particle size (Fig. 12D) both made by Pacific Particulate Material Ltd. Canada. Two types of polycrystalline 40–50 μm diamond particles with 30 and 56 wt% nickel coating (shown in Fig. 12E and F for 30% with 5.13 g/cm^3 density and 56% with 6.53 g/cm^3 density, respectively) were provided by Van Moppes & Sons Ltd. from Switzerland.

In Table 1 a list of equipment to fabricate the samples is given. To test the proposed fabrication technology six materials were manufactured. The details on the composition (in grams and wt%) is given in Table 2. Note that only samples No.5 and No.6 contain a 316 L lattice with 5 wt% diamond (15 mm height and 20 mm diameter, 1 mm lattice cell size), and the rest of them are lattice-free. Mixing Ti6Al4V (low-density titanium alloy), which has high strength and high corrosion resistance, with 316 L (high-density steel alloy), which has high ductility, produces a resistant composite that can be subjected to relatively high strain and an abrasive medium at high temperatures. In the current paper, 316 L-diamond FGL with circumferential to longitudinal 1:1 ratio of unit cell size in bottom, 1:2 in middle, and 1:3 for top is applied for samples No.5 and No.6. The tribological tests were carried out with

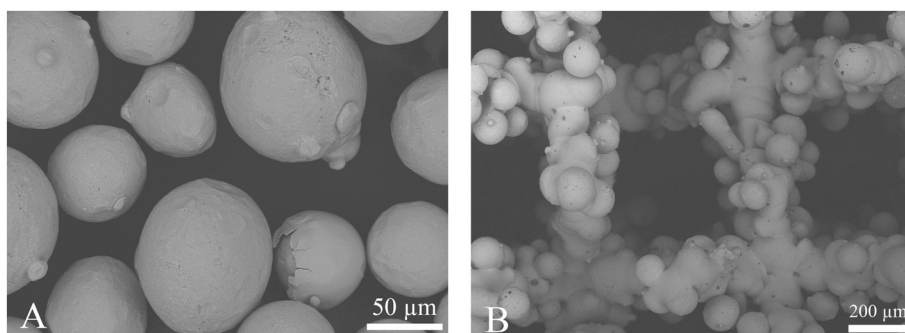


Fig. 5. Rockit 701 (Fe balance with 9.5 wt% W). A) Particles and B) 3D printed structure with unit cell size of 1 mm and smallest thickness of strut.

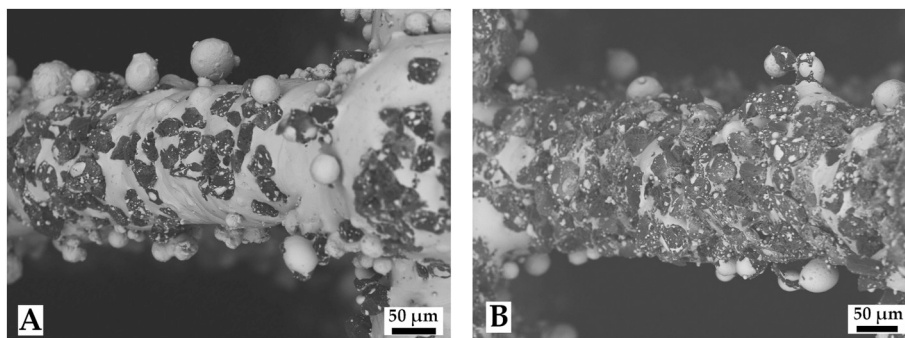


Fig. 6. 3D printed Ti6Al4V lattice structure with A) 5% and B) 10% diamond of volume content. The unit cell size is 1 mm and strut diameter 0.2 mm in both cases (top view).

1:1 cell size side.

Two steps of the SPS procedure included pre-heating/drying at 260 °C, 10 MPa, 6 min and sintering at 860 °C, 100 MPa, 6 min (see Fig. 13). Pre-heating (drying) step helps to dry the powders to avoid later surface oxidation of nickel coating and results in better bonding between the diamond particle and metals. The selected parameters of sintering were the maximum possible. The increase of the temperature and pressure in the sintering step above 860 °C and 100 MPa was leading to squeezing of melted metals (Ni, Cr, and Mo) out of the mold of the SPS machine.

The set parameters of the 3D metal printer were: laser current 3000 mA, exposure time 600 μs, and point distance of 1 μm. Note that the same printing parameters can be used to print both, 316 L and Ti6Al4V powders. Fig. 14A and B shows the difference between 316 L lattice and 316 L with 5% nickel-coated diamond particles. Diamond printing without considerable change to graphite phase is facilitated by pre-heating step, the close melting point of nickel and steel, and uniform distribution of diamond particles; whereas, excellent consolidation of the composite for the impact-abrasive application depends on SLM parameters (laser current, exposure time, point distance) and SPS parameters (pressure, temperature, time). Consolidated diamond particles in surrounded metal powders after SPS is shown in Fig. 15A and B with different magnifications for sample No.1. As well, embedded lattice structures of the sample No.5 is shown in Fig. 16.

The wear resistance evaluation of specimens to simulate excavation in mines and tunnels was performed on the innovative impact-abrasive tribological device (IATD, it is shown in Fig. 17A) developed at Tallinn University of Technology [37]. The impact loading was performed with the energy of impact 5.6 J and frequency of impact 28 Hz by Makita hammer drill. The WC-15% Co wheel with 100 mm diameter, 8 mm wide and 1 m/s sliding speed is pressed against specimen with 49 N force. Specimens after sintering were having the following dimensions: diameter - 20 mm and height - 10 mm (Fig. 17B). Abrasive sand grain

size 0.2–0.3 mm were flowing through a nozzle into the wear region (between the wheel and specimen surface) with 200 g/min rate. An optical surface profiler (OSP) was applied to characterize the results after 5 min (300 m sliding distance) of impacting and abrading with IATD.

3. Results and discussion

The results of the impact/abrasive test on the IATD are presented in Fig. 18 for the six samples from Table 2. The volumetric wear rates were measured three times and averaged. Significantly different results are obtained for each type of composite. It is demonstrated that samples No.3 (lattice-free) and No.6 (lattice-included) have superior wear resistance (both samples are visualized via OSP analyzer in Fig. 19). This can be attributed to the presence of Cr, Ni, Mo, Al, and V elements in the mix of 316 L and Ti6Al4V powders which even promotes the excellent mechanical properties. Additional Cr and Mo in samples No.2 made it more wear resistant than No.1 (Fig. 18). Another vital factor was a balance between the diamond percentage and that of bonding metals. It means that No.3 is more abrasion resistant than No.4 because of equilibrium between Cr-Mo-Ni and Diamond. For example, Cobalt alloy CoCr28Mo6 has higher hardness (HV10–385) and ductility than Ti6Al4V (HV10–370), 316 L (HV10–210) or nickel alloy IN939 (HV10–305) [8]. The idea of adding extra Cr–Mo to Ni has been raised to make the composite harder, more ductile and providing enough metal matrix for better performance of diamond particles.

316 L-5 wt% nickel-diamond SLM lattice can be adopted as an impact absorber structure that is sintered, filled in SPS along with other powders. No. 1–4 have 16 g weight and can be compared in pairs (pair one: No.1 and 2; pair two: No.3 and 4) due to almost equal amount of diamond. While, No.5 and 6 have 19 g weight and equal lattice structure. Nevertheless, it was not an unexpected outcome that sample No.6 wear resistance is better than No.5, because of a higher volume of

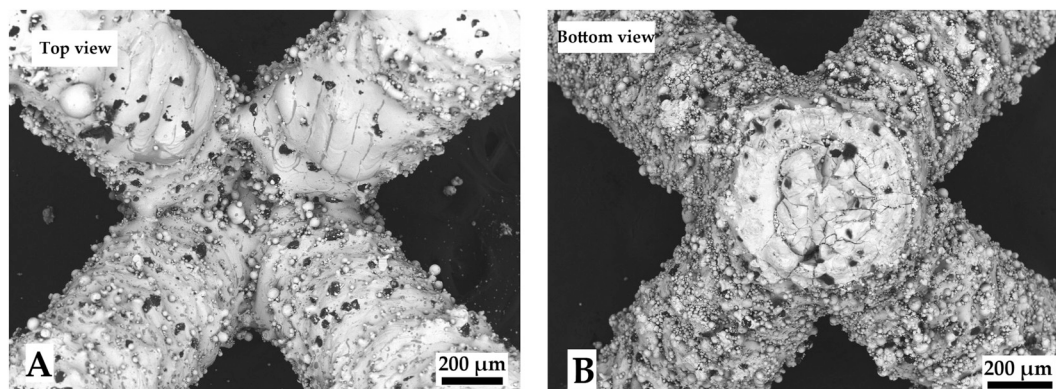


Fig. 7. 3D printed Ti6Al4V lattice structure with 5% diamond. A) Top and B) Bottom view. The unit cell size is 2 mm and the strut diameter is 0.5 mm.

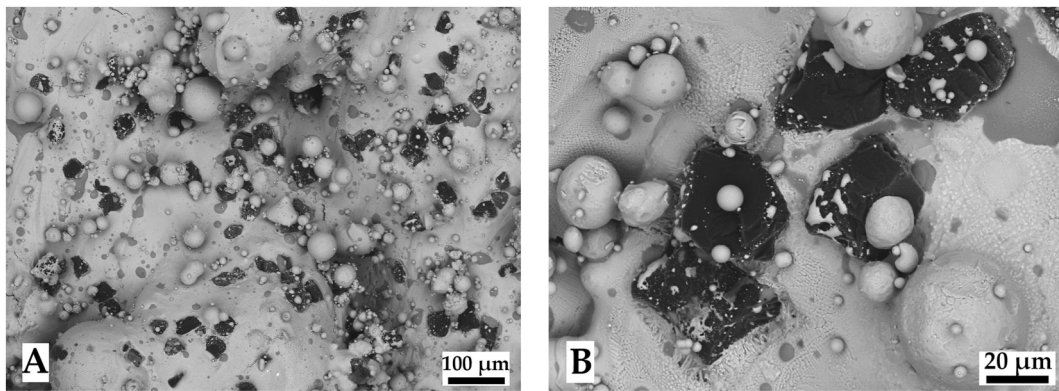


Fig. 8. 3D printed Ti6Al4V bulk volume with 5 wt% diamond. A) X500 and B) X1000 magnification. The specimen was 20 mm in diameter and 5 mm in height.

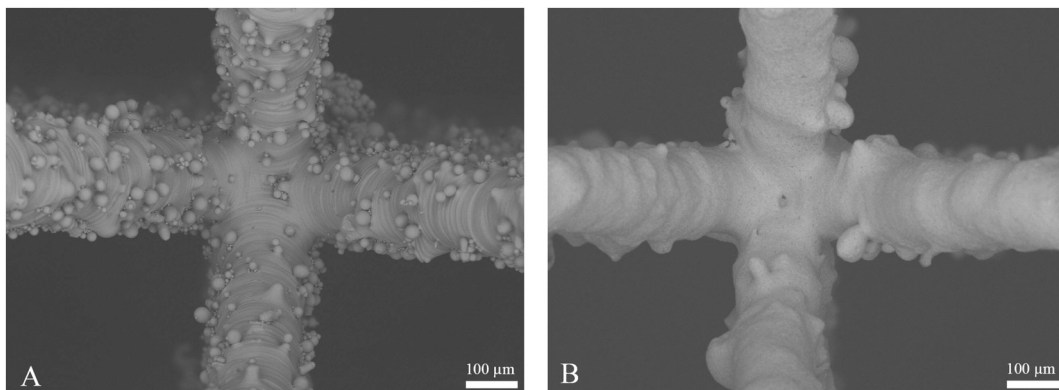


Fig. 9. Ti6Al4V lattice structures with 1.5 mm cell size and 0.2 mm strut diameter A) after printing and B) after alumina nanoparticle blasting.

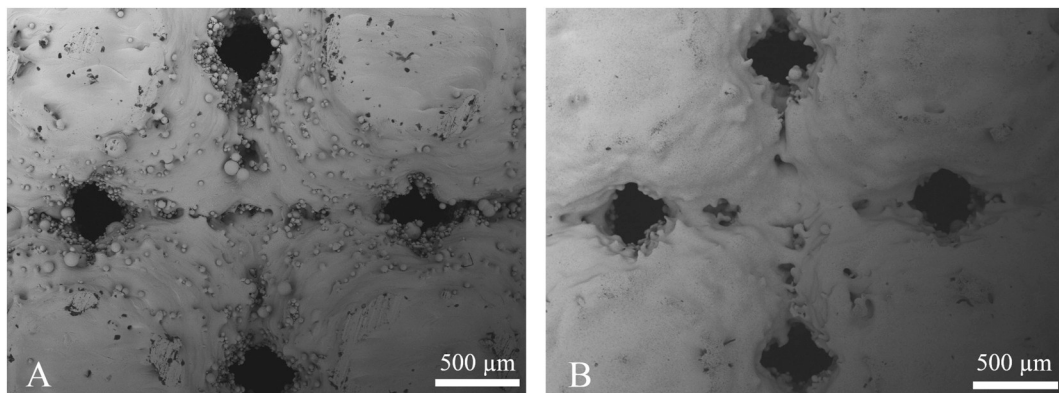


Fig. 10. Ti6Al4V lattice structures with 2.0 mm cell size and 1 mm strut diameter A) after printing and B) after alumina nanoparticle polishing.

diamond, a better balance between the value of Cr-Mo-Ni and proper bonding between melted lattice and sintered powders which is suitable for improving wear resistance, impact energy absorption and damage tolerance. Micrographs of samples after IATD is shown in Fig. 19. However, depth of wear scar in No.3 can be more in some points because of brittle fracturing but has lower volume of material lost during test. In equal test conditions, the wear scar of sample No.6 is more “flat” while wear of sample No.3 material is “cylindrical” (similar to the shape of the wheel of tribodevice). This is because of ductility of the lattice structure that was trapping diamond particles and removing them uniformly.

Fig. 20A demonstrates the distribution of diamond, titanium, iron, and nickel as EDS color mapping of sample No.3. The EDS elemental mapping results of 316 L, Ti6Al4V and diamond nickel-coating composition (without lattice) illustrated the presence of 12 elements,

namely, C 46.44%, Ti 23.31%, Fe 12.15%, Ni 9.65%, Cr 3.82%, Al 1.44%, V 1.11%, P 0.75%, Sn 0.52%, Mn 0.36%, Si 0.30%, and S 0.15% (Diamond with nickel coating usually contains small amount of phosphorus and chromium [38]). Also, the EDS elemental mapping results for Ti6Al4V and diamond nickel-coating composition embedded in 316 L lattice showed presence of 14 elements, namely, C 47.27%, Ti 23.57%, Fe 9.36%, Ni 8.40%, Al 3.36%, Cr 2.91%, Si 1.20%, V 1.04%, P 0.79%, W 0.60%, Na 0.43%, S 0.35%, Ca 0.34%, and Mn 0.30% (Fig. 20B).

In the current case, better weldability (or ability to be tightly fixed by bolts without brittle fracturing) at the bottom (more metal) and better abrasive behavior (more hard material) at the top is targeted for mining applications. Another advantage of using metallic cellular lattice was better electrical conductivity for materials during SPS process to gain more consolidated/densified composition with lower

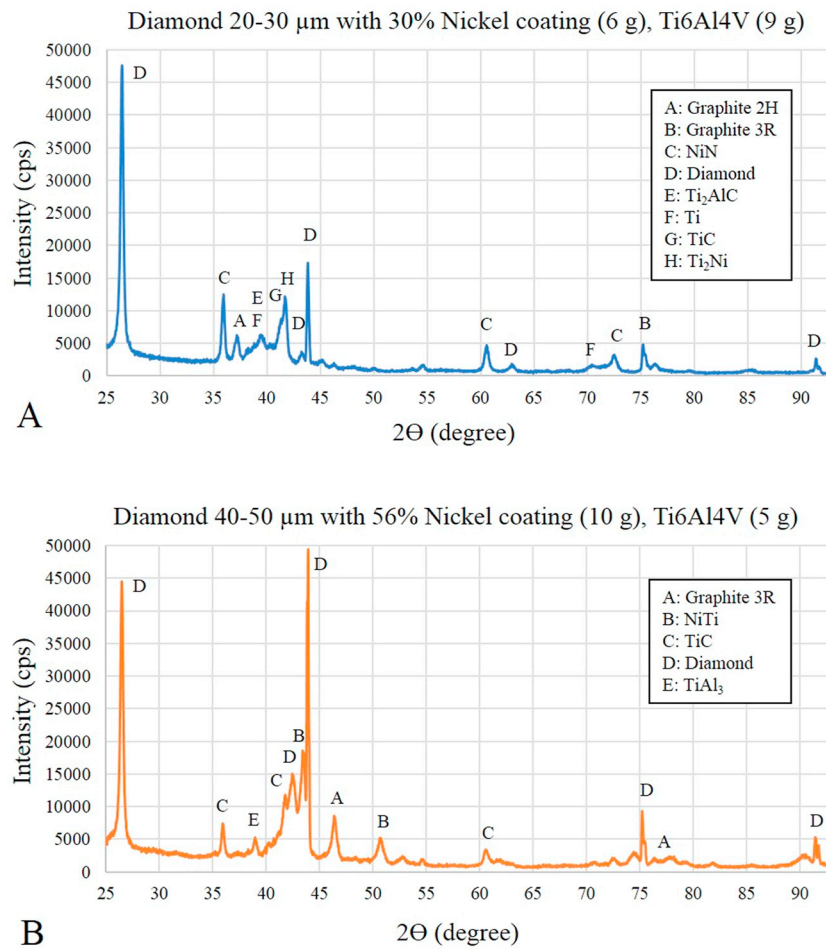


Fig. 11. XRD diffraction comparison of diamond-nickel-Ti6Al4V with different constituent volume. A) Diamond size 20–30 μm with 30% Nickel coating (6 g), Ti6Al4V (9 g), B) Diamond size 40–50 μm with 56% Nickel coating (10 g), Ti6Al4V (5 g).

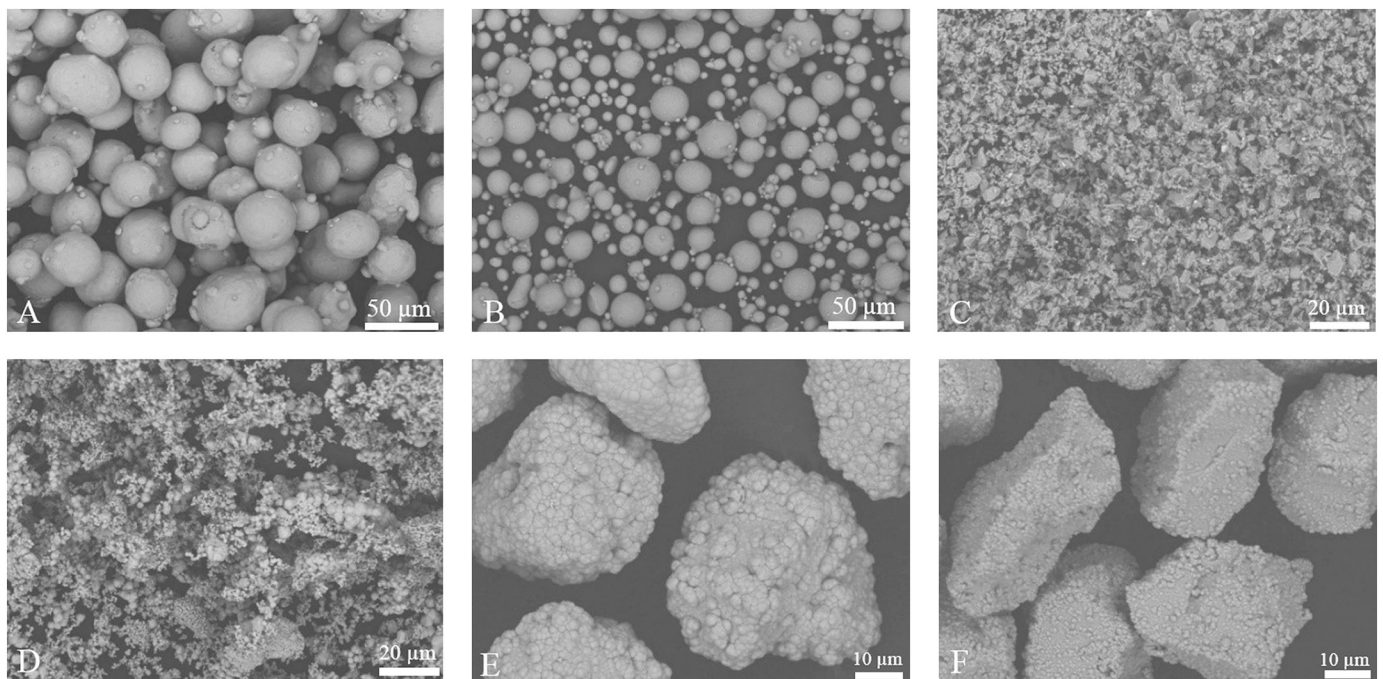


Fig. 12. SEM images of A) 316 L, B) Ti6Al4V, C) Chromium, D) Molybdenum, E) Diamond-56 wt% Ni, and F) Diamond-30 wt% Ni.

Table 1
Used machines list.

Process	Machine, specification
Selective Laser Melting (SLM)	Realizer SLM50, construction volume $\varnothing 70 \times 40$ mm, layer thickness 20–50 μm
Spark Plasma Sintering (SPS)	FCT System, up to 2200 °C and 100 MPa, 1000 °C/min heating rate
Impact-abrasive tribo-device (IATD)	Tribosystem, up to 19 J impact energy and up to 55 Hz impact frequency
Vacuum Nitriding Furnace (VNF)	R. D. WEBB, up to 1700 °C, nitrogen flow and 10 °C/min heating rate
Scanning Electron Microscopy (SEM)	Hitachi TM-1000, magnification 20–10,000 X
3D Optical Surface Profiler (OSP)	Bruker ContourGT-K0+, lost volume calculation from millimeter to nanometer range
Energy-dispersive Spectroscopy (EDS)	Zeiss EVO MA15 SEM with INCA Energy 350 X-ray micro-analyzer

Table 2

Description of samples content (in units of gram) - Lattice structures with 1 mm cell size are printed from 95 wt. % 316 L and 5 wt% of “Diamond-56 wt. % Ni”. Average particle sizes are: diamond 40–50 μm , Ti6Al4V 5–40 μm , 316 L 30–55 μm .

No.	Diamond (56 wt. % Ni)	Diamond (30 wt. % Ni)	Ti6Al4V	316 L	Chromium	Molybdenum	Lattice
1	8		4	4			
2	8		3.5	3.5	0.5	0.5	
3		6	5	5			
4		6	4.5	4.5	0.5	0.5	
5	8		3	3	0.5	0.5	4
6		6	4	4	0.5	0.5	4

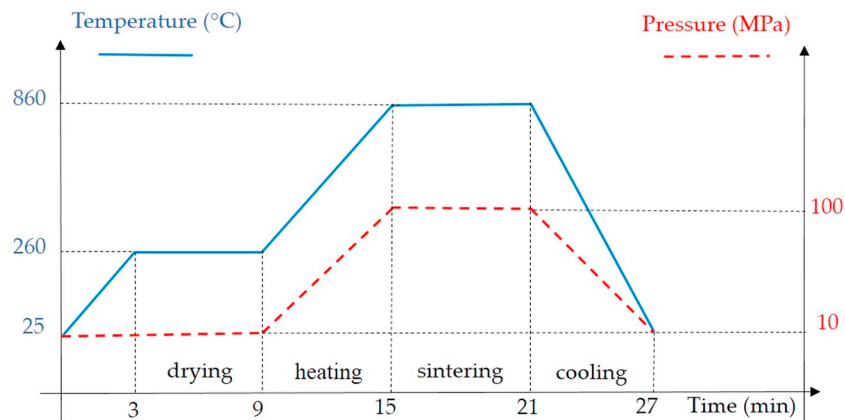


Fig. 13. SPS pressure-temperature sequence.

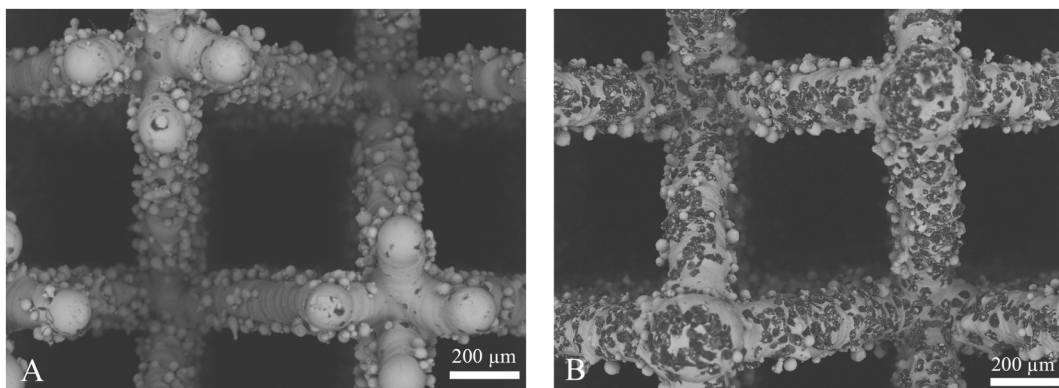


Fig. 14. SEM micrographs of A) 316 L and B) 316 L-5% diamond lattices (after 3D printing).

temperature and electric current. This method is advantageous to avoid material wasting in unnecessary surfaces/volumes and making higher performance cutters and blades by reduction the cost and time required for exchange operations. Depending on the volume fraction of the samples, three types of lattices were suggested in this paper: low, average and high as shown in Fig. 4. The low 12% volume fraction lattice structure (unit cell size 1.5 mm, Fig. 4A) did not lead to an expected increased wear resistance and noticeable damage tolerance. On

the other hand, the high 26% volume fracture lattice (unit cell size 0.75 mm, Fig. 4C) reduced the diamond content in the mixture, resulting in a decrease in hardness and wear resistance. The 19% volume fraction lattice (unit cell size 1 mm, Fig. 4B), combining 316 L and 5 wt % diamond mixed powder had the best properties.

The addition of chromium, molybdenum and nickel to the iron-based or titanium-based alloys improve corrosion, wear, chemical and heat resistance that is useful in medical and food industries [39,40].

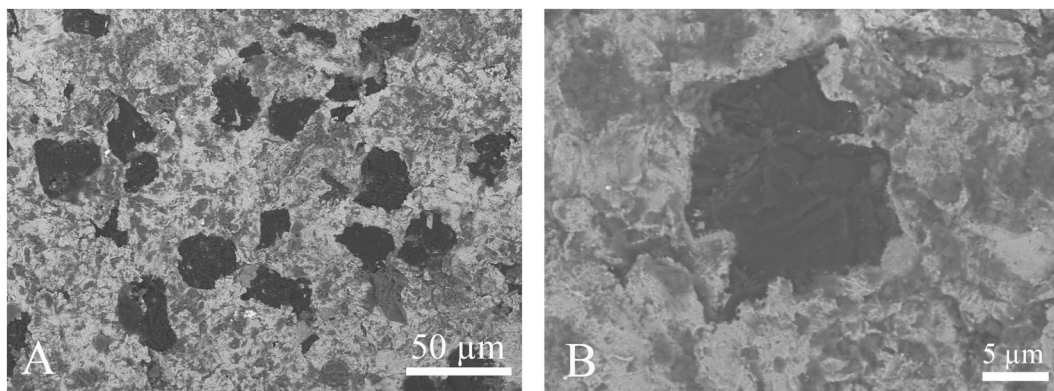


Fig. 15. SEM micrographs of sintered sample No.1 A) 500 ×, B) 2000 × (after SPSing).

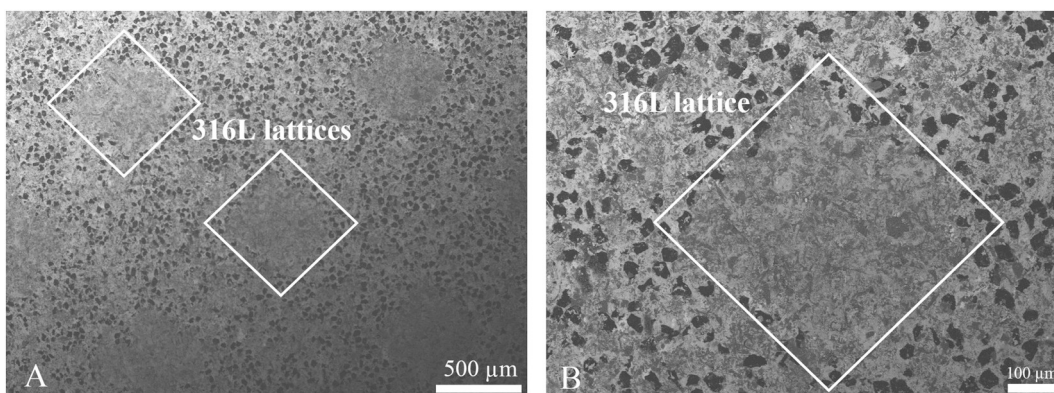


Fig. 16. SEM micrographs of sample No.5, lattice included (after SPSing).

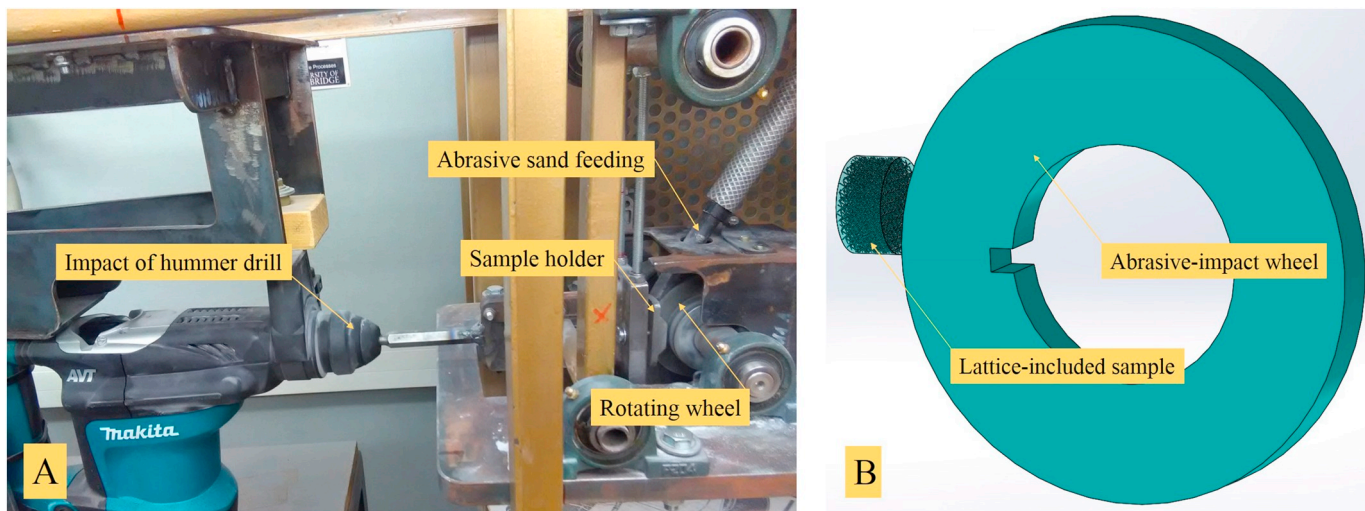


Fig. 17. A) Impact-abrasive tribology device (IATD) developed at Tallinn University of Technology, B) Lattice-included sample designed by SolidWorks.

However, nickel coating naturally has 8–12 wt% of phosphorus (producer company data [38]). As expected, sample No.2 is exhibited better wear resistance than No.1 (56% Ni coating for both samples No.1 and No.2), because increase of Cr–Mo, increases wear resistance. For the same reason, sample No.3 is evaluated higher impact-abrasive resistance than No.4 (30% Ni coating for both samples No.3 and No.4). Therefore, finding a balance point between diamond particles and bonding metals is necessary, because Cr-Mo-Ni increasing more than a critical value make it less resistant against impact and abrasion.

4. Simulation and application

To model the impact-abrasive conditions and to provide the tool for analysis and optimization of the relevant materials for these and other similar applications, the coupling of SolidWorks (CAD design) and Comsol (nonlinear dynamic analysis) was performed [24]. In the current simulation, the same dimensions were set up for both cylindrical samples (Ø 20 × 10 mm) under single impact test without abrasive particles (Fig. 17). Mesh configuration is shown in Fig. 21. A finer mesh was chosen in the lattice structure as compared to the abrasive wheel. The numerical test was modeled in only one-stroke and in uniaxial

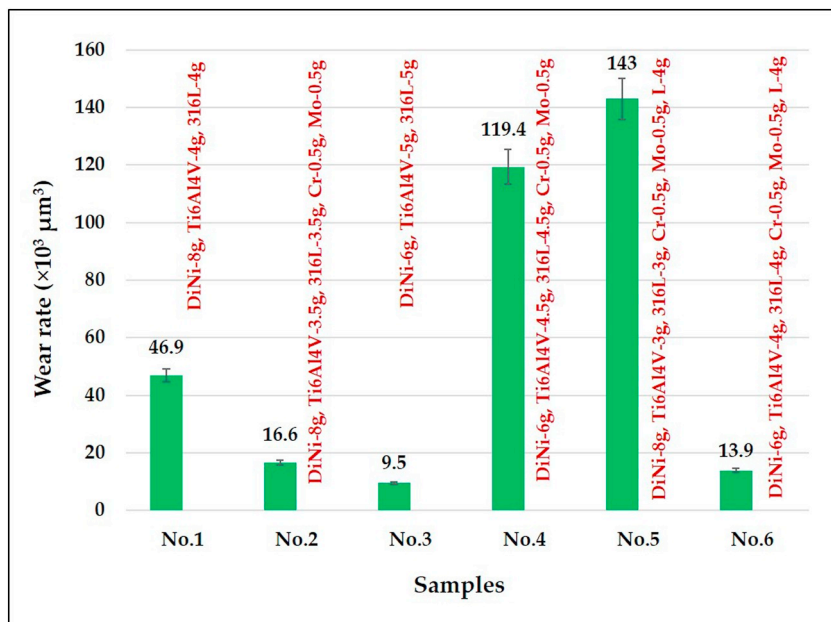


Fig. 18. Wear rate of samples during impact-abrasive test measured by 3D OSP (Di = diamond, Ni = nickel, Cr = chromium, Mo = molybdenum, and L = lattice).

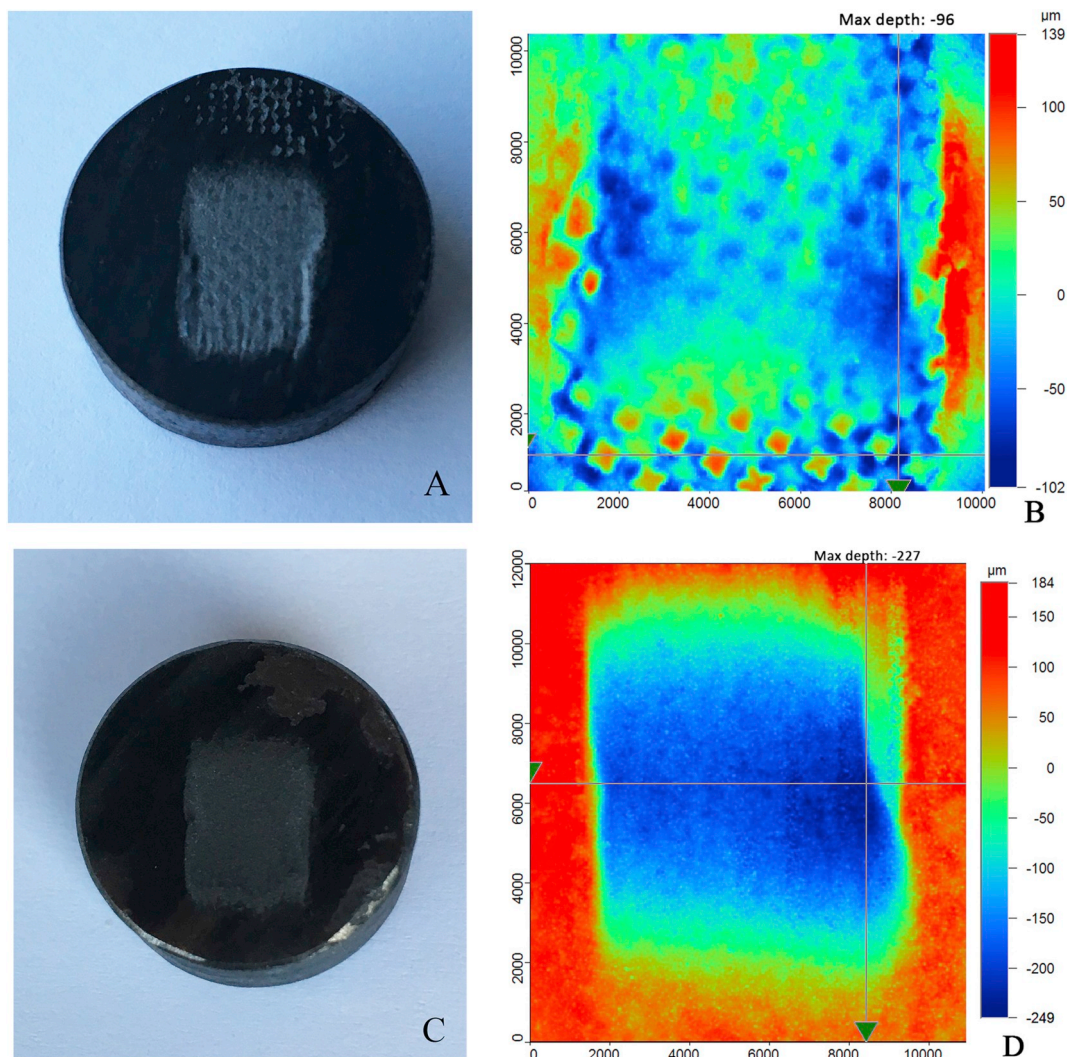


Fig. 19. Image of samples A) No.6 and C) No.3, OSP contour micrograph of samples B) No.6 and D) No.3 after impact-abrasive test (dimensions of lattice structures are 20 mm diameter and 9 mm height).

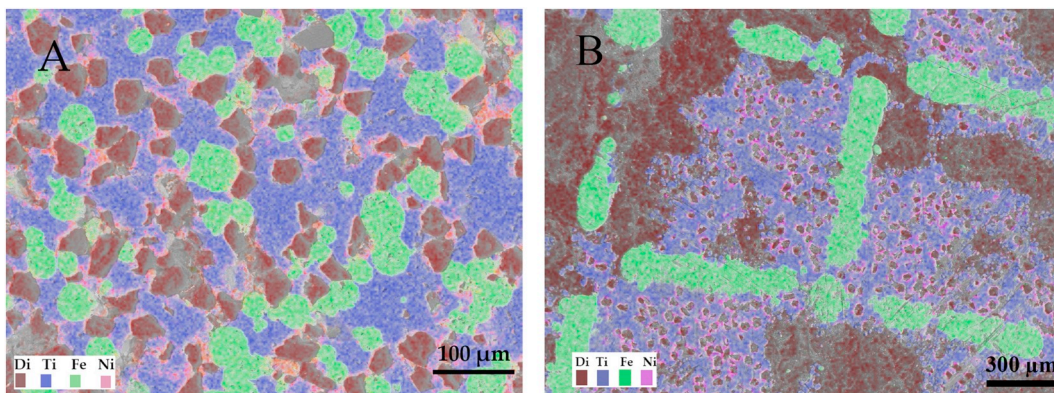


Fig. 20. EDS color mapping of A) 316 L, Ti6Al4V and diamond nickel-coating composition (without lattice) B) Ti6Al4V and diamond nickel-coating composition embedded in 316 L (with lattice).

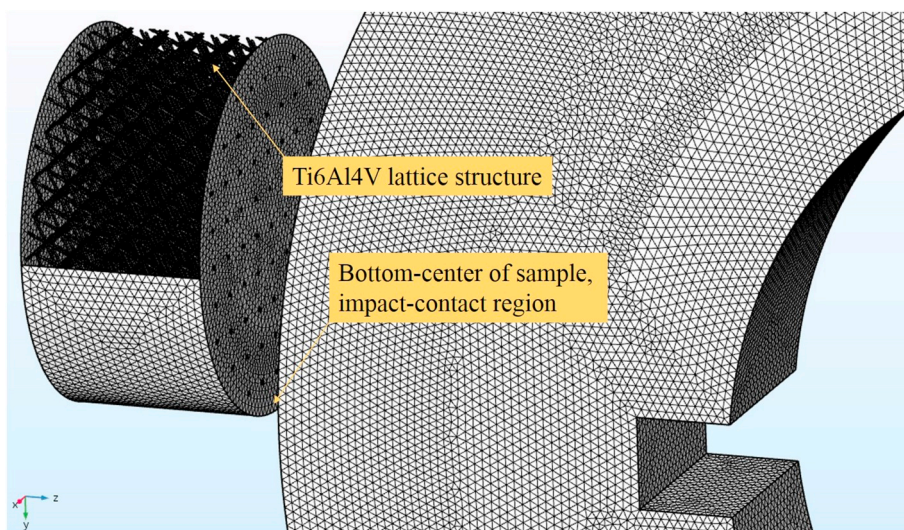


Fig. 21. Mesh configuration by Comsol based on tribo-device for impact test.

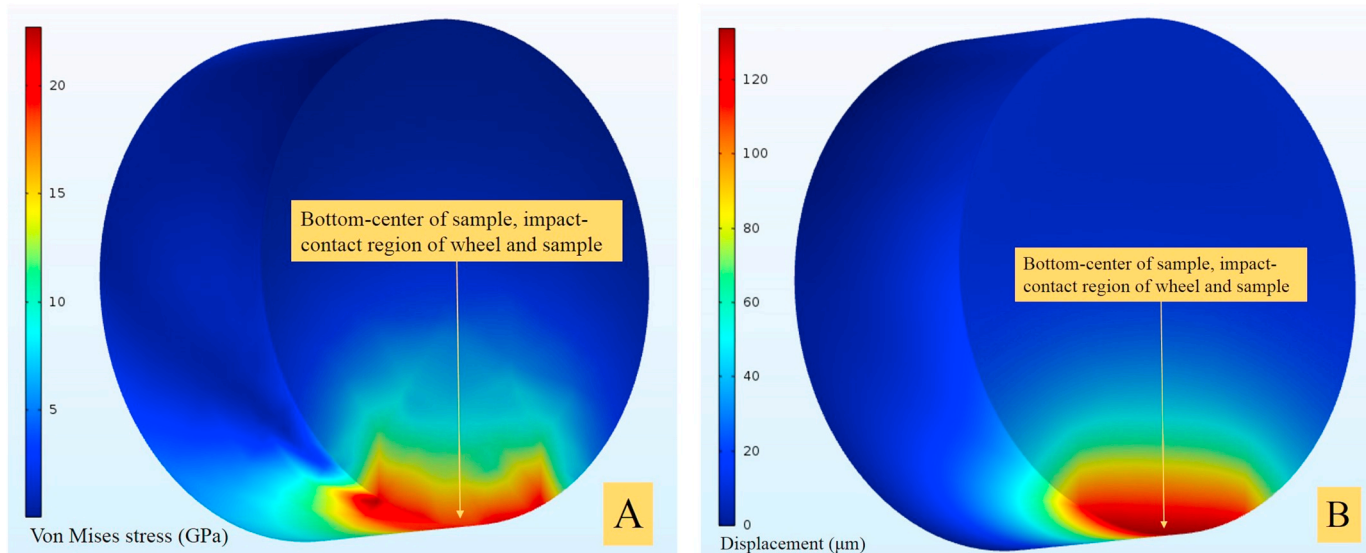


Fig. 22. Stress distribution and deformation of simple sample (pure diamond) after impact test (test 1).

direction with 5.6 J impact energy (non-rotating wheel, Ø 100 diameter). In the first simulation, a bulk specimen made from pure diamond was tested. The results for the Von Mises stress and displacement

is illustrated in Fig. 22. As expected, maximum values of stress and deformation are measured at the contact of the wheel and the sample. The simulation yielded maximum ≈ 23 GPa of stress and ≈ 135 μm

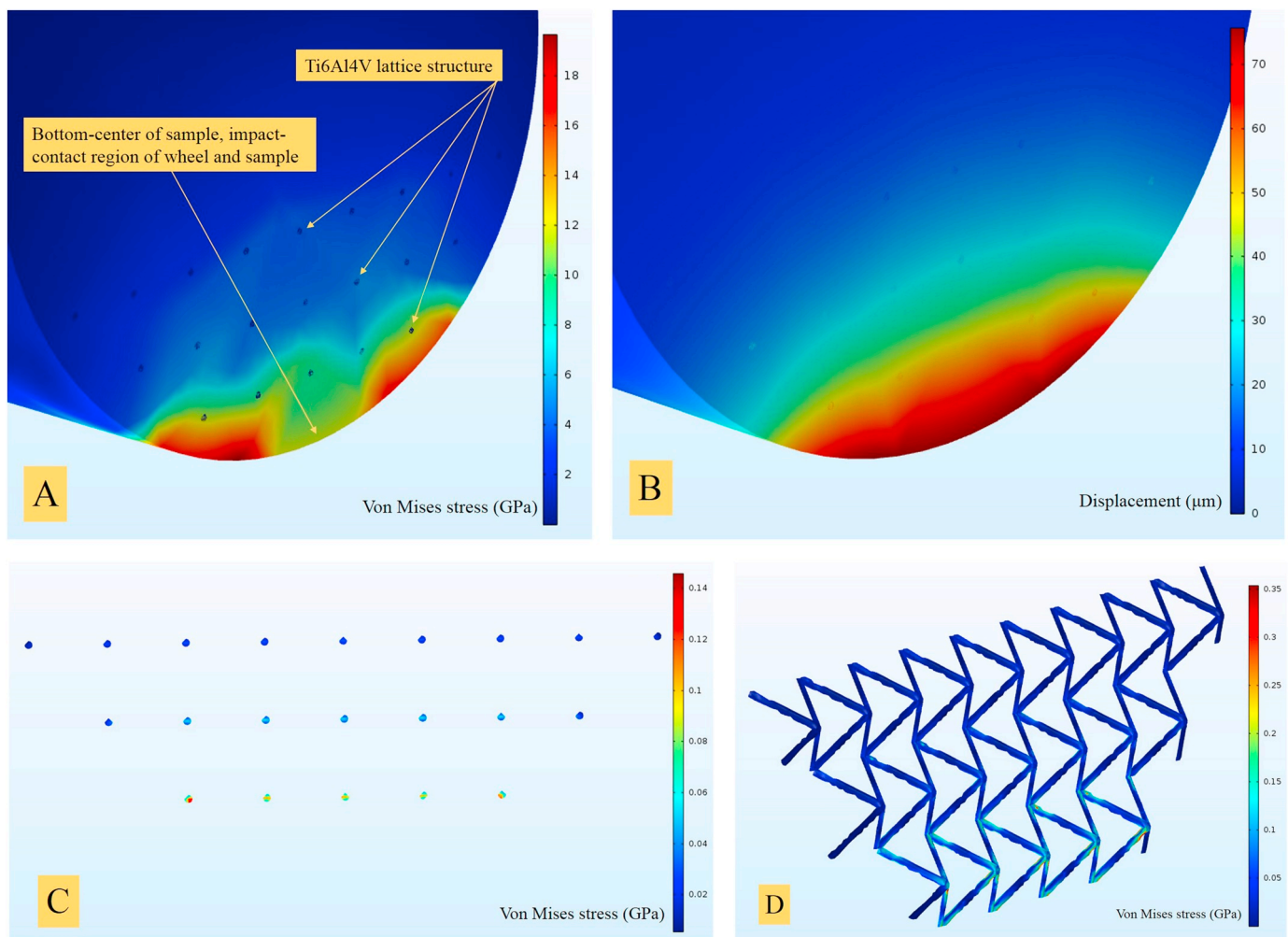


Fig. 23. Stress distribution and deformation of 316 L-lattice included (lattice beams have 0.2 mm diameter) diamond sample after impact test with impact influence on three bottom rows of lattice structure (test 2).

maximum displacement. The second test was modeled 2 mm unit cell size 316 L lattice structure throughout the sample (Fig. 23). The results (stress max. ≈ 19 GPa and displacement max. ≈ 75 μm) demonstrate impact absorption by 316 L lattices and significantly decrease in deformation of the sample. The presence of embedded lattice structure (uniform or gradient) prevents the increase of stress (Figs. 22A and 23A) and works as an impact absorber due to the lateral deformability of continuous metallic structure.

5. Conclusion

A new route has been introduced to fabricate parts with increased wear and impact resistance for the use in tunneling and mining applications. We used SPS method to consolidate metal-diamond composite having lattice structures manufactured by the SLM. The lattices can include diamond particles or other hard materials. Mixed 316 L-Ti6Al4V binder alloys and Cr-Mo-Ni transition metals made a strong additive composition for consolidation diamond particles in situ. 3D printing of functionally gradient lattice structures by SLM, nitriding, chromium coating, blasting by alumina jet, diamond mixing to 316 L particles in the SLM process of making lattices, and diamond mixing to Ti6Al4V in the SPS process of filling the lattice, were used in this paper. It was shown that adding 10 wt% coated diamond particles in the 316 L or Ti6Al4V powders results in slightly brittle scaffolds (in comparison to e.g. 5 wt% diamond) because of the weaker intersection and junction of struts due to less amount of binding metal. In addition, our tests show

that during solid/plain printing of Ti6Al4V-diamond mixture, the diamond particles are agglomerated at the bottom layers during 3D printing because of difference in shape, size and density. Our design by functionally gradient lattice in three stages enables better weldability/ductility at the bottom (where more metal is concentrated) and better hardness at the top (where more hard material can be located). Generally, positional definition of metal-diamond composition in desired location (continuous change from 100% metal to almost 100% hard reinforcement in uniaxial direction) in the FGL structure can be achieved with the proposed technology. Laboratory experiments of wear/impact on an impact-abrasive tribology device, developed in-house, were performed. The results show that the balance of nickel, molybdenum, and chromium in the content affects the performance of the fabricated specimens. Adding a higher content of Mo-Cr into Ni guarantees higher impact-abrasive resistance of the composite, along with the diamond particles coated by 30% Ni. A balance content between diamond powders and bonding metals (Cr, Mo and Ni) is important in both lattice-free and lattice-included structure types. We also performed finite element simulations which show that metallic-printed lattice structures enable more uniform distribution of stresses throughout the volume of the sample which implies that such structures have promising properties for applications e.g. in drilling/mining for their impact absorption abilities.

Different produced additive manufacturing powders (with spherical shapes) can be considered to mix with diamond or other hard materials (such as c-BN or WC-Co) as binder metal alloy powders include Ni-

based (Inconel625 or Inconel718), Co-based (CoCrMo or CoCrW), or Fe-based (high toughness 1.2709 or high tensile strength 1.4542). As current research has targeted the future of 3D printing on tunneling application with developed impact/abrasion test machine, it is desirable to investigate on geothermal earth drilling with emphasis on fatigue/rotating test machine and proper lattice structures. A circumferential FGL can be suggested with a metallic cylindrical core in the center and radially increased hard material from innermost to outermost diameter.

Declaration of Competing Interest

The authors (Ramin Rahmani, Miha Brojan, Maksim Antonov, and Konda Gokuldoss Prashanth) declare that there are no conflicts of interest regarding the publication of "Perspectives of metal-diamond composites additive manufacturing using SLM-SPS and other techniques for increased wear-impact resistance" in Journal of "International Journal of Refractory Metals & Hard Materials".

Acknowledgments

This research was supported by the Estonian Ministry of Higher Education and Research under Projects (IUT19-29 and ETAG18012), project number 2014-2020.4.01.16-0183 (Smart Industry Centre), Slovenian Research Agency (Program P2-0263), European Regional Funds through the project MOBERC15 and TTÜ base finance project (B56 and SS427). The authors would like to thank *Rainer Traksmaa* for the help with XRD patterning, *Heinar Vagiström* for the help with surface cleaning of samples via alumina nanoparticles and *Mart Viljus* for the help with EDS mapping.

References

- [1] Y. Holovenko, L. Kollo, M. Saarna, R. Rahmani, T. Soloviova, M. Antonov, K.G. Prashanth, S. Cygan, R. Veinthal, Effect of lattice surface treatment on performance of hardmetal-titanium interpenetrating phase composites, *Int. J. Refract. Met. Hard Mater.* 86 (2020) 105087.
- [2] R. Rahmani, M. Antonov, L. Kollo, Wear resistance of (diamond-Ni)-Ti6Al4V gradient materials prepared by combined selective laser melting and spark plasma sintering techniques, *Adv. Tribol.* (2019) 5415897.
- [3] <https://setis.ec.europa.eu/>.
- [4] www.hoganas.com/surface-coating.
- [5] Y. Holovenko, M. Antonov, L. Kollo, I. Hussainova, Friction studies of metal surfaces with various 3D printed patterns tested in dry sliding conditions, *Proce. Instit. Mech. Eng. Part J: J. Eng. Tribol.* 232 (2018) 43–53.
- [6] K.G. Prashanth, J. Eckert, Formation of metastable cellular microstructures in selective laser melted alloys, *J. Alloys Compd.* 707 (2017) 27–34.
- [7] E. Louvis, P. Fox, C.J. Sutcliffe, Selective laser melting of aluminium components, *J. Mater. Process. Technol.* 211 (2011) 275–284.
- [8] <https://www.slm-solutions.com/en/products/>.
- [9] A. Strondl, O. Lyckfeldt, H. Brodin, U. Ackelid, Characterization and control of powder properties for additive manufacturing, *springer, JOM* 67 (2015).
- [10] K.G. Prashanth, R. Damodaram, T. Maity, P. Wang, J. Eckert, Friction welding of selective laser melted Ti6Al4V parts, *Mater. Sci. Eng. A* 704 (2017) 66–71.
- [11] K.G. Prashanth, S. Kolla, J. Eckert, Additive manufacturing processes: selective laser melting, electron beam melting and binder jetting-selection guidelines, *Materials* 10 (2017) 672.
- [12] K. Dash, B.C. Ray, D. Chaira, Synthesis and characterization of copper-alumina metal matrix composite by conventional and spark plasma sintering, *J. Alloys Compd.* 516 (2012) 78–84.
- [13] V. Mamedov, Spark plasma sintering as advanced PM sintering method, *Powder Metall.* 45 (2002) 322–328.
- [14] <http://www.fct-systeme.de/en>.
- [15] A.B. Spierings, M. Voegtlin, T. Bauer, K. Wegener, Powder flowability characterisation methodology for powder-bed based metal additive manufacturing, *Progr. Addit. Manuf.* (2016) 9–20.
- [16] H. Galarraga, R.J. Warren, D.A. Lados, R.R. Dehoff, M.M. Kirka, P. Nandwana, Effects of heat treatments on microstructure and properties of Ti-6Al-4V ELI alloy fabricated by electron beam melting (EBM), *Mater. Sci. Engin. A* 685 (2017) 417–428.
- [17] C. Yan, L. Hao, A. Hussein, D. Raymont, Evaluations of cellular lattice structures manufactured using selective laser melting, *Int J Mach Tool Manu* 62 (2012) 32–38.
- [18] J. Ping Li, J.R. de Wijn, C.A. Van Blitterswijk, K. de Groot, Porous Ti6Al4V scaffold directly fabricated by rapid prototyping: preparation and in vitro experiment, *Biomaterials* 27 (2006) 1223–1235.
- [19] Z.H. Liu, D.Q. Zhang, S.L. Sing, C.K. Chua, L.E. Loh, Interfacial characterization of SLM parts in multi-material processing: metallurgical diffusion between 316L stainless steel and C18400 copper alloy, *Mater. Charact.* 94 (2014) 116–125.
- [20] F. Velasco, W.M. Lima, N. Anton, J. Abenojar, J.M. Torralba, Effect of intermetallic particles on wear behaviour of stainless steel matrix composites, *Tribol. Int.* 36 (2003) 547–551.
- [21] A. Buford, T. Goswami, Review of wear mechanisms in hip implants: paper I-general, *Mater. Des.* 25 (2004) 385–393.
- [22] US9302945B2 United States Patent, 3-D Diamond Printing Using a Pre-Ceramic Polymer With A Nanoparticle Filler, <https://patents.google.com/patent/US9302945B2/en>.
- [23] R. Rahmani, M. Antonov, L. Kollo, Selective laser melting of diamond-containing or postnitrided materials intended for impact-abrasive conditions: experimental and analytical study, *Adv. Mater. Sci. Eng.* (2019) 4210762.
- [24] R. Rahmani, M. Antonov, N. Kamboj, Modelling of impact-abrasive wear of ceramic, metallic, and composite materials, *Proc. Est. Acad. Sci.* 68 (2019) 191–197.
- [25] R.M. Hooper, J.L. Henshall, A. Klopfer, The wear of polycrystalline diamond tools used in the cutting of metal matrix composites, *Int. J. Refract. Met. Hard Mater.* 17 (1999) 103–109.
- [26] J.P. Davim, Diamond tool performance in machining metal-matrix composites, *J. Mater. Process. Technol.* 128 (2002) 100–105.
- [27] E.A. Ekimov, N.V. Suetin, A.F. Popovich, V.G. Raichenko, Thermal conductivity of diamond composites sintered under high pressures, *Diam. Relat. Mater.* 17 (2008) 838–843.
- [28] V.V.N. Reddy, B. Ramamoorthy, P.K. Nair, A study on the wear resistance of electrodeless Ni-P/diamond composite coatings, *Wear* 239 (2000) 111–116.
- [29] X. Wan, A. Hu, M. Li, C. Chang, D. Mao, Performances of CaSiO₃ ceramic sintered by spark plasma sintering, *Mater. Charact.* 59 (2008) 256–260.
- [30] N. Kamboj, M.A. Rodriguez, R. Rahmani, K.G. Prashanth, I. Hussainova, Bioceramic scaffolds by additive manufacturing for controlled delivery of the antibiotic vancomycin, *Proc. Est. Acad. Sci.* 68 (2019) 185–190.
- [31] R. Rahmani, M. Rosenberg, A. Ivask, L. Kollo, Comparison of mechanical and antibacterial properties of TiO₂/Ag ceramics and Ti6Al4V-TiO₂/ag composite materials using combining SLM-SPS techniques, *Metals* 9 (2019) 874.
- [32] R. Rahmani, M. Antonov, Y.H. Kollo, K.G. Prashanth, Mechanical behavior of Ti6Al4V scaffolds filled with CaSiO₃ for implant applications, *Appl. Sci.* 9 (2019) 3844.
- [33] Y. Holovenko, L. Kollo, M. Jöeleht, R. Ivanova, T. Soloviova, R. Veinthal, Production of metal-ceramic lattice structures by selective laser melting and carburizing or nitriding, *Proc. Est. Acad. Sci.* 68 (2019) 131–139.
- [34] S. Van Bael, Y.C. Chai, S. Truscello, M. Moesen, G. Kerckhofs, H. Van Oosterwyck, J.-P. Kruth, J. Schrooten, The effect of pore geometry on the in vitro biological behavior of human periosteum-derived cells seeded on selective laser-melted Ti6Al4V bone scaffolds, *Acta Biomater.* 8 (2012) 2824–2834.
- [35] S. Barui, S. Chatterjee, S. Mandal, A. Kumar, B. Basu, Microstructure and compression properties of 3D powder printed Ti-6Al-4V scaffolds with designed porosity: experimental and computational analysis, *Mater. Sci. Eng. C* 70 (2017) 812–823.
- [36] J.M. Sobral, S.G. Caridade, R.A. Sousa, J.F. Mano, R.L. Reis, Three-dimensional plotted scaffolds with controlled pore size gradients effect of scaffold geometry on mechanical performance and cell seeding efficiency, *Acta Biomater.* 7 (2011) 1009–1018.
- [37] M. Antonov, R. Veinthal, D.-L. Yung, D. Katusin, I. Hussainova, Mapping of impact-abrasive wear performance of WC-co cemented carbides, *Wear* 332–333 (2015) 971–978.
- [38] <http://www.vanmoppes.ch/en/>.
- [39] B.F. Shahgaldi, F.W. Heatley, A. Dewar, B. Corrin, In vivo corrosion of cobalt-chromium and titanium wear particles, *J. Bone Joint Surg.* 77 (1995).
- [40] E. Zhumelzu, I. Goyos, C. Cabezas, A. Opitz, A. Parada, Wear and corrosion behaviour of high-chromium (14-30% Cr) cast iron alloys, *J. Mater. Process. Technol.* 128 (2002) 250–255.